Articles

Structural and Kinetic Characterization of Active-Site Histidine as a Proton Shuttle in Catalysis by Human Carbonic Anhydrase II[†,‡]

Zoë Fisher,[§] Jose A. Hernandez Prada,[§] Chingkuang Tu,[||] David Duda,[§] Craig Yoshioka,[§] Haiqian An,[||] Lakshmanan Govindasamy,[§] David N. Silverman,*[,||] and Robert McKenna*[,§]

Departments of Biochemistry and Molecular Biology and of Pharmacology and Therapeutics, College of Medicine, University of Florida, Gainesville, Florida 32610

Received September 13, 2004; Revised Manuscript Received November 8, 2004

ABSTRACT: In the catalysis of the hydration of carbon dioxide and dehydration of bicarbonate by human carbonic anhydrase II (HCA II), a histidine residue (His64) shuttles protons between the zinc-bound solvent molecule and the bulk solution. To evaluate the effect of the position of the shuttle histidine and pH on proton shuttling, we have examined the catalysis and crystal structures of wild-type HCA II and two double mutants: H64A/N62H and H64A/N67H HCA II. His62 and His67 both have their side chains extending into the active-site cavity with distances from the zinc approximately equivalent to that of His64. Crystal structures were determined at pH 5.1−10.0, and the catalysis of the exchange of ^{18}O between CO_2 and water was assessed by mass spectrometry. Efficient proton shuttle exceeding a rate of 10^5 s^{-1} was observed for histidine at positions 64 and 67; in contrast, relatively inefficient proton transfer at a rate near 10^3 s^{-1} was observed for His62. The observation, in the crystal structures, of a completed hydrogen-bonded water chain between the histidine shuttle residue and the zinc-bound solvent does not appear to be required for efficient proton transfer. The data suggest that the number of intervening water molecules between the donor and acceptor supporting efficient proton transfer in HCA II is important, and furthermore suggest that a water bridge consisting of two intervening water molecules is consistent with efficient proton transfer.

Carbonic anhydrase II is one of the most efficient of the isozymes of the α-class of anhydrases (*1*, *2*). The enzymes in the family of carbonic anhydrases are zinc metalloenzymes that catalyze the hydration of carbon dioxide to produce bicarbonate and a proton. The catalytic mechanism can be described in two separate and distinct parts (*1*−*3*).

$$EZn{-}OH^- + CO_2 \rightleftarrows EZn{-}HCO_3^- \overset{H_2O}{\rightleftharpoons} EZn{-}H_2O + HCO_3^- \quad (1)$$

$$B + EZn{-}H_2O \rightleftarrows B + {}^+H{-}EZn{-}OH^- \rightleftarrows BH^+ + EZn{-}OH^- \quad (2)$$

The first step is the hydration of CO_2 by the zinc-bound OH^-, followed by the displacement of a HCO_3^- ion by water (eq 1). The second step is the deprotonation of the zinc-bound water to regenerate the zinc-bound OH^-; here B is a proton acceptor that is a buffer in solution or part of the enzyme itself. His64 in CA II acts as a proton shuttle between the zinc-bound solvent and buffer in solution (eq 2). Mutation of His64 to an alanine reduces enzymatic activity 10−50-fold (*4*), and it has been postulated that the proton transfer between the zinc-bound water and His64 occurs through intervening water molecules (*1*−*5*).

In wild-type human carbonic anhydrase II (HCA II),[1] proton transfer between the side chain of His64 and the zinc-bound solvent molecule proceeds during catalysis at a rate as great as 10^6 s^{-1} (*1*−*3*). Our current understanding of the requirements for rapid proton transfer in carbonic anhydrase involves several aspects that could be elucidated by comparisons of kinetics and structure. There is current interest in the function of a hydrogen-bonded water chain, or proton wire, as a pathway for the proton transfer. Recent calculations indicate that this proton transfer probably has a significant component that is concerted and involves tunneling (*6*, *7*). The number of water molecules involved in proton transfer and the distance between the proton donor and acceptor are

[†] This work was supported in part by the University of Florida, College of Medicine, start-up funds (R.M.), the Thomas Maren Foundation (R.M.), and National Institutes of Health Grant GM25154 (D.N.S.).

[‡] The atomic coordinates have been deposited in the Protein Data Bank (entries 1T9N, 1TBO, 1TBT, 1TE3, 1TEQ, 1TEU, 1TG3, 1TG9, 1TH9, and 1THK).

* To whom correspondence should be addressed. R.M.: Department of Biochemistry and Molecular Biology, College of Medicine, University of Florida, Box 100245, Gainesville, FL 32610; phone, (352) 392-5696; fax, (352) 392-3422; e-mail, rmckenna@ufl.edu. D.N.S.: Department of Pharmacology, College of Medicine, University of Florida, Box 100267, Gainesville, FL 32610; phone, (352) 392-3556; fax, (352) 392-9696; e-mail, silvermn@college.med.ufl.edu.

[§] Department of Biochemistry and Molecular Biology.

[||] Department of Pharmacology and Therapeutics.

[1] Abbreviations: HCA II, human carbonic anhydrase II; H64A, His64 mutated to Ala; MES, 2-(*N*-morpholino)ethanesulfonic acid; CAPS, 3-(cyclohexylamino)-1-propanesulfonic acid; EXAFS, extended X-ray absorption fine structure.

10.1021/bi0480279 CCC: $30.25
Published on Web 01/05/2005

important considerations. The analysis of free energy plots suggests that there is a significant unfavorable pre-equilibrium that precedes a very rapid proton transfer in carbonic anhydrase; this may involve the formation of a hydrogen-bonded water chain and orientation of the side chain of the proton donor His64 (*8*). Finally, the shuttling of protons between the solution and the zinc-bound solvent molecule may require some conformational mobility of the side chain of His64 as the proton donor or acceptor. Evidence for this comes from crystal structures in which proton shuttle residue His64 in HCA II (*9*) and Glu84 in the archaeal carbonic anhydrase from *Methanosarcina thermophila* (*10*, *11*) exhibit two conformational rotamers in the active-site cavity. A chemically modified cysteine residue acting as a proton shuttle in a mutant of CA V also shows evidence of multiple orientations (*12*).

Kinetic analysis of wild-type HCA II over the pH range of 6.0−9.0 shows that HCA II is active over a broad pH range (*13*, *14*). Also, structural analysis of wild-type HCA II at pH 5.7 and 6.5 showed that the active site exhibits no major pH-dependent conformational changes, with the exception of proton shuttle residue His64 (*9*). The position of His64 occupies a conformation oriented away from the zinc ion at pH 5.7 and is named the "out" conformation, while at pH 8.5, the side chain of His64 is in the "in" conformation, pointing toward the zinc ion. The positions of these two pH-dependent conformations (in and out) of His64 are related as side chain torsion angle rotamers of χ_1 (*9*). The experimentally determined pK_a of His64 in wild-type HCA II is 7.1 (*15*), and therefore, the imidazole side chain of this residue would be positively charged at pH 5.7. The conformation of His64 in the out conformation at pH 5.7 is possibly due to electrostatic repulsion between the positively charged imidazolium group and the positive charge of the tetrahedrally coordinated zinc ion. In contradiction to this rationale, it has been observed that His64 in the mutant T200S HCA II was in the out conformation at pH 8.0 (*16*).

The kinetic significance of the location of the histidine proton shuttle has been studied by introducing histidine residues at different positions in the active-site cavity of HCA II (*17*) and HCA III (*18*). These results show that a histidine residue at sites other than position 64 is able to participate in proton transfer; specifically, His67 appears to be capable of more efficient proton transfer than His62.

We have studied the crystal structures of wild-type HCA II as well as HCA II mutants H64A/N62H and H64A/N67H under a wide range of pH conditions, and we have assessed the exchange of ^{18}O between CO_2 and water catalyzed by these enzymes to determine what common structural features are important for proton transfer. In these examples, the distance between the donor and acceptor appears to be more significant for efficient proton transfer than the observation of a completed, hydrogen-bonded water chain in the crystal structure. These data suggest that in HCA II two intervening water molecules between the donor and acceptor are consistent with an efficient proton transfer.

EXPERIMENTAL PROCEDURES

Enzymes. Plasmids with the appropriate mutations in the cDNA of HCA II were provided by S. Lindskog (Umeå University, Umeå, Sweden). Wild-type HCA II and the mutants H64A/N62H and H64A/N67H were expressed and purified by affinity chromatography (*19*).

Crystallography. Crystals of wild-type and mutant HCA II were obtained using the hanging drop method (*20*). The crystallization drops were prepared by mixing 5 μL of protein [concentration of 10.5 mg/mL in 50 mM Tris-HCl (pH 7.8)] with 5 μL of the precipitant solution [50 mM Tris-HCl (pH 7.8) and 2.5−2.9 M ammonium sulfate] at 4 °C against 600 μL of the precipitant solution. Useful crystals were observed 5 days after the crystallization setup. The pH values of the wild-type crystals were obtained by equilibrating crystals in appropriate buffers (50 mM sodium acetate at pH 5.1, 50 mM MES at pH 6.1, 50 mM Tris-HCl at pH 7.0, 7.8, and 9.3, and 50 mM CAPS at pH 10.0) and 3.0 M ammonium sulfate. The pH values of the double mutant crystals were obtained by using the same approach described above using the buffers (50 mM Tris-HCl at pH 6.0 and 7.8) and 3.0 M ammonium sulfate. Crystals were allowed to equilibrate for 4−12 h at 4 °C before data collection to ensure complete solvent exchange in the crystal lattice (the pH stated was that measured at the start of the experiment).

X-ray diffraction data sets were obtained using an R-AXIS IV++ image plate system with Osmic mirrors and a Rigaku HU-H3R Cu rotating anode operating at 50 kV and 100 mA. The detector to crystal distance was set to 100 mm for H64A/N67H and 120 mm for H64A/N62H and wild-type HCA II X-ray data collection. Each data set was collected at room temperature from a single crystal mounted in a quartz capillary. The oscillation steps were 1° with a 3 min exposure per image. X-ray data processing was performed using DENZO and scaled and reduced with SCALEPACK (*21*). All models were built using O, version 7 (*22*). Refinement was carried out with CNS, version 1.1 (*23*). The wild-type HCA II structure [Protein Data Bank entry 2CBA (*24*)], which was isomorphous with all the data sets collected, was used to phase the data sets. To avoid phase bias of the model, the zinc ion, mutated side chains, and water molecules were removed. After one cycle of rigid body refinement, annealing by heating to 3000 K with gradual cooling, geometry-restrained position refinement, and temperature factor refinement, the $2F_o - F_c$ Fourier maps were generated. These density maps clearly showed the position of the zinc and the mutated residues, which were subsequently built into the respective models. After several cycles of refinement, solvent molecules were incorporated into the models using the automatic water-picking program in CNS until no more water molecules were found at a 2.0σ level. Refinement of the models continued until convergence of R_{cryst} and R_{free} was reached.

^{18}O Exchange. This method is based on the assessment by membrane-inlet mass spectrometry of the exchange of ^{18}O between CO_2 and water at chemical equilibrium (*25*) (eqs 3 and 4).

$$HCOO^{18}O^- + EZnH_2O \rightleftarrows EZnHCOO^{18}O^- \rightleftarrows COO + EZn^{18}OH^- \quad (3)$$

$$EZn^{18}OH^- + BH^+ \rightleftarrows EZnH_2{}^{18}O + B \overset{H_2O}{\rightleftharpoons} EZnH_2O + H_2{}^{18}O + B \quad (4)$$

An Extrel EXM-200 mass spectrometer with a membrane-inlet probe was used to measure the isotopic content of CO_2.

Table 1: Crystallography Data and Refinement Statistics for Wild-Type, H64A/N62H, and H64A/N67H HCA II at Different pHs

HCA II[a]	resolution (Å)	no. of unique reflections	completeness (%)	R_{symm} (%)	R_{cryst}/R_{free} (%)	average B (Å^2) (main chain/side chain)	average B for solvent (Å^2)	no. of solvent molecules
WT, pH 5.1	2.00	15898	93.1	6.3	19.5/20.9	16.14/20.33	27.79	112
WT, pH 6.1	2.00	16365	95.9	12.0	14.5/20.5	22.93/26.82	30.37	91
WT, pH 7.0	2.00	15878	93.5	5.1	13.0/18.4	18.16/22.15	27.72	112
WT, pH 7.8	2.00	16212	95.1	7.3	12.8/20.1	14.42/18.32	27.02	150
WT, pH 9.0	2.00	16751	98.6	9.2	13.4/17.3	17.01/21.03	27.74	112
WT, pH 10.0	2.00	16714	97.8	8.1	13.43/17.53	17.11/21.16	27.90	115
H64A/N62H, pH 6.0	1.80	22162	95.0	7.4	17.1/20.6	16.35/19.84	29.54	129
H64A/N62H, pH 7.8	1.90	18130	91.8	7.2	16.8/21.7	16.49/19.67	28.57	137
H64A/N67H, pH 6.0	1.63	29130	93.5	5.9	17.8/21.0	17.15/20.76	30.59	120
H64A/N67H, pH 7.8	1.80	21547	92.7	6.8	16.6/20.9	15.77/19.37	29.29	132

[a] The rms deviations of bond lengths and angles were between 0.038 and 0.005 Å and between 1.3° and 2.1°, respectively. Ramachandran statistics for all amino acids were ~90% in most favored and ~10% in additionally allowed regions with none in disallowed regions.

Solutions contained a total concentration of all species of CO_2 of 25 mM unless otherwise indicated.

This approach yields two rates for the ^{18}O exchange catalyzed by carbonic anhydrase. The first is R_1, the rate of exchange of CO_2 and HCO_3^- at chemical equilibrium, as shown in eq 5.

$$R_1/[E] = k_{cat}^{ex}[S]/(K_{eff}^{S} + [S]) \quad (5)$$

where k_{cat}^{ex} is a rate constant for maximal interconversion of substrate and product, K_{eff}^{S} is an apparent binding constant for substrate to enzyme, and [S] is the concentration of substrate, either CO_2 or bicarbonate. The k_{cat}^{ex}/K_{eff}^{S} ratio is, in theory and in practice, equal to k_{cat}/K_m obtained by steady-state methods. The binding of CO_2 and HCO_3^- to the active site of carbonic anhydrase is weak (*26*), and in this work, $[CO_2] \ll K_{eff}^{S}$. The pH dependence of k_{cat}/K_m depends on the ionization state of the zinc-bound water, as shown in eq 6.

$$k_{cat}/K_m = (k_{cat}/K_m)_{max}(1 + [H^+/(K_a)_{ZnH_2O})^{-1} \quad (6)$$

A second rate determined by the ^{18}O exchange method is R_{H_2O}, the rate of release from the enzyme of water bearing substrate oxygen (eq 4). This is the component of the ^{18}O exchange that is enhanced by exogenous proton donors (*25*). The pH dependence of $R_{H_2O}/[E]$ is often bell-shaped, consistent with the transfer of a proton from a single predominant donor to the zinc-bound hydroxide. In these cases, the pH profile is adequately fit by eq 7 in which k_B is a pH-independent rate constant for proton transfer, and $(K_a)_{donor}$ and $(K_a)_{ZnH_2O}$ are the noninteracting ionization constants of the proton donor BH^+ of eq 4, the zinc-bound water.

$$k_B^{obs} = k_B/\{[1 + (K_a)_{donor}/[H^+]][1 + [H^+]/(K_a)_{ZnH_2O}]\} \quad (7)$$

RESULTS

Crystallography. All crystals were isomorphous and belonged to space group $P2_1$ with the following mean unit cell dimensions: $a = 42.7 \pm 2.0$ Å, $b = 41.6 \pm 1.0$ Å, $c = 72.9 \pm 2.0$ Å, and $\beta = 104.6 \pm 2.0°$. The HCA II wild-type data sets were processed to 2.0 Å resolution, while the mutant data sets ranged from 1.8 to 1.6 Å resolution. A summary of the data set statistics is given in Table 1.

A least-squares superimposition of the wild-type HCA II structures (at pH 5.1, 6.1, 7.0, 9.0, and 10.0) onto the pH 7.8 structure revealed no significant variation between them (average rms deviations of 0.10 Å, for all atoms). Similar analysis of the mutant structures (H64A/N62H at pH 6.0 and 7.8 and H64A/N67H at pH 6.0 and 7.8) showed an average rms deviation of 0.15 Å compared with the pH 7.8 wild-type HCA II structure. When the two double mutants were compared to each other, the average rms deviation was 0.07 Å.

Effect of pH on the Wild-Type HCA II Active Site. The structural integrity of the tetrahedral coordination of the zinc ion by His94, His96, His119, and the zinc-bound solvent molecule was unchanged over the broad pH range (pH 5.1−10.0, Figure 1). The displacement of the zinc-bound water by an oxygen of a sulfate molecule at pH 5.1 had little to no observable effect on the tetrahedral coordination of the zinc ion (Figure 1A) at 2.0 Å resolution. A conserved, ordered water network that bridges the zinc-bound solvent molecule and the proton shuttle, His64, was observed in all the structures at pH 6.1−10.0. This consisted of two water molecules (W1 and W2; Figure 1 and Table 2); however, the distances from W2 to the imidazole side chain of His64 were too long at all values of pH for a viable hydrogen bond (Table 2). Two additional water molecules were also conserved in wild-type structures, flanking each side of water molecule W2 (W3A and W3B; Figure 1 and Table 2). This configuration creates the possibility of two alternative water pathways leading from the zinc-bound solvent molecule to His64 (W1−W2−W3A−His64 or W1−W2−W3B−His64); again, the distances from W3A or W3B to the side chain of His64 were too long for a hydrogen bond (Table 2).

The only experimentally observable difference between wild-type structures over the pH range was the positional occupancy of the side chain of His64 (Figure 1). The occupancies of His64 for each structure were determined from calculated $F_o - F_c$ electron density maps, where His64, W1, W2, W3A, and W3B were omitted to prevent model bias. The residual density volumes were used to determine the relative occupancies of the in and out His64 conformers. At pH 6.1, 7.0, and 7.8, the occupancies were 60, 70, and 80% in the in conformation, respectively (Figure 1B,C; pH 7.8 data not shown), while at pH 9.0 and 10.0, the occupancy remained 80% in the in conformation (Figure 1D). These values show that as the pH increased from 6.1 to 10.0 the occupancy of His64 favored the in conformation, consistent

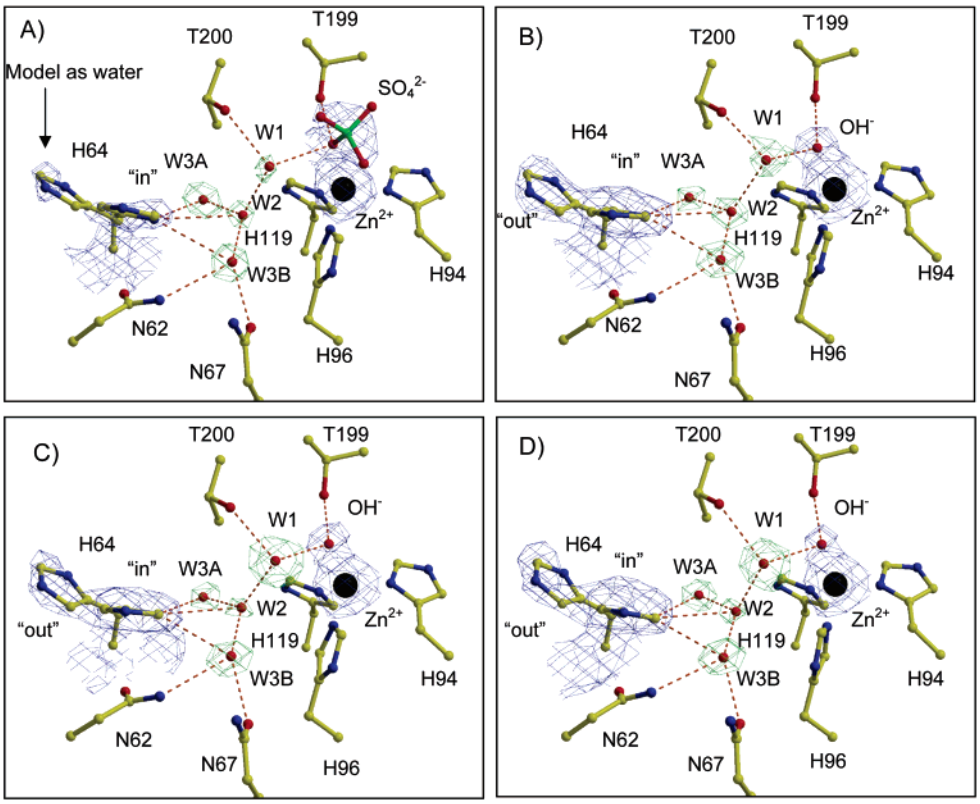

FIGURE 1: Crystal structures of the wild-type human CAII active site. Panels A−D are shown in the same orientation at (A) pH 5.1, (B) pH 6.1, (C) pH 7.0, and (D) pH 10.0. Electron density maps ($2F_o - F_c$) are shown. Water molecules and SO_4^{2-} are contoured at 1.5σ and are colored green and blue, respectively; His64 in and out conformers are contoured at 1.0σ and are colored blue, and the Zn^{2+} is contoured at 3.0σ and colored blue. Red dashed lines connect ordered solvent and residues but do not indicate hydrogen bonds (see Table 2 for distances). This figure was generated and rendered using BobScript and Raster3D (*34*, *35*).

Table 2: Heavy Atom Distances (in angstroms) Connecting Zinc-Bound Solvent (or sulfate) and Proton Shuttles in Wild-Type, H64A/N62H, and H64A/N67H HCA II

structure	Zn−Zn-bound ion[a]	Zn-bound ion[a]−W1	W1−W2	W2−W3A	W2−W3B	W2−His64[b]	W3A−His64[b]	W3B−His64[b]	W2−His67	W3B−His62
WT, pH 5.1	1.99	3.10	2.84	2.70	2.83	3.58	3.46	3.79	–	–
WT, pH 6.1	2.01	2.54	3.02	2.82	2.77	3.51	3.54	3.60	–	–
WT, pH 7.0	2.03	2.56	2.79	2.74	2.66	3.35	3.46	3.59	–	–
WT, pH 7.8	2.14	2.63	2.67	2.87	2.80	3.54	3.52	3.34	–	–
WT, pH 9.0	2.01	2.75	2.74	2.81	2.76	3.47	3.45	3.66	–	–
WT, pH 10.0	1.98	2.75	2.73	2.85	2.72	3.31	3.40	3.54	–	–
H64A/N62H, pH 7.8	2.06	3.12	2.34	2.88	2.51	–	–	–	–	3.21
H64A/N67H, pH 7.8	2.08	2.86	2.90	2.97	2.94	–	–	–	3.19	–

[a] Zn-bound ion is SO_4^{2-} for WT at pH 5.1 and an H_2O/OH^- for all other structures. [b] His64 is given as the in conformation (Figures 1 and 2). The structural geometries of H64A/N62H and H64A/N67H at pH 6.0 are not shown as they have sulfate bound in the active site.

with the work of Nair and Christianson (*9*). However, in the case of pH 5.1 at which a sulfate molecule was bound to the zinc, the His64 side chain is 90% in the in conformation (Figure 1A). This orientation of the imidazolium side chain of His64 may be influenced by electrostatic attraction to the Zn-bound SO_4^{2-}.

Effect of pH on the Double Mutant HCA II Active Sites. The protein−solvent and solvent−solvent hydrogen bond networks in the active site for the double mutants H64A/N62H and H64A/N67H HCA II are different from each other. Even though the mutant active sites are solvated in a manner similar to that of the wild-type structures, the water molecules have been reorganized compared to wild-type HCA II (Figures 2 and 3 and Table 2). It is notable that H64A/N62H and H64A/N67H have a SO_4^{2-} bound to the metal at pH 6.0, an anion that displaces the zinc-bound solvent molecule (Figures 2A and 3A), similar to that observed for wild-type HCA II at pH 5.1 (Figure 1A). The structures of H64A/N62H and H64A/N67H at pH 7.8 show no sulfate and have a solvent molecule bound at the zinc ion (Figures 2B and 3B). In the case of H64A/N62H at pH 7.8, the zinc-bound solvent molecule is linked to His62 by a network of three water molecules (W1−W2−W3B, Figure 2B). In this case, a completed hydrogen-bonded bridge is observed between His62 and the zinc-bound solvent, as estimated by solvent distance geometries (Table 2), although the hydrogen bond to His62 by W3B is rather weak based on the length of the bond. In the case of H64A/N67H at pH 7.8, there are two water molecules connecting the zinc-bound solvent to His67 (W1−W2, Figure 3B), and again, the distance geometries are appropriate for implying a completed hydrogen-bonded bridge (Table 2). This network of two water molecules, between the proton donor and acceptor, is the same as seen for the wild type at pH 6.1−10.0 (Figure

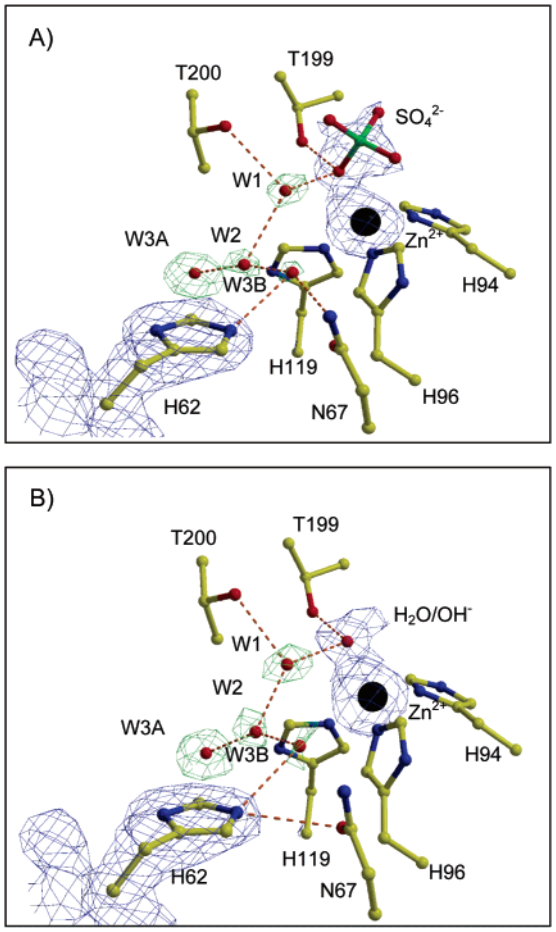

FIGURE 2: Crystal structure at the active site of double mutant H64A/N62H HCA II shown in the same orientation as Figure 1 at (A) pH 6.0 and (B) pH 7.8. Electron density maps ($2F_o - F_c$) are shown. Other details are as described for Figure 1.

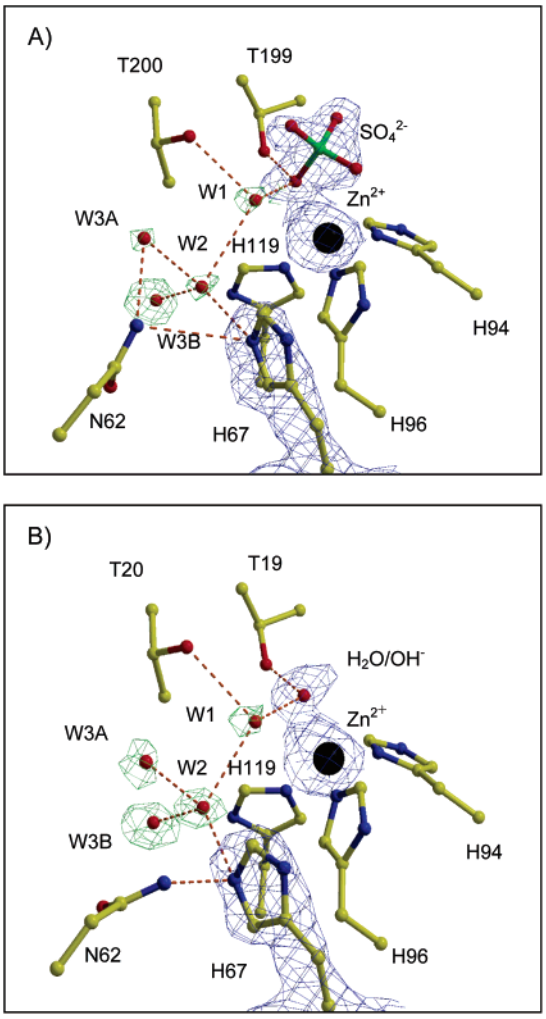

FIGURE 3: Crystal structure at the active site of double mutant H64A/N67H HCA II shown in the same orientation as Figure 1 at (A) pH 6.0 and (B) pH 7.8. Other details are as described for Figure 1.

1), except in the case of the wild type, the hydrogen-bonded chain is incomplete.

Catalysis. The pH dependence of R_{H_2O}/[E], the proton transfer-dependent rate constant for release of $H_2{}^{18}O$ from the active site, was measured for the enzymes of this study. Wild-type HCA II and each of the two double mutants of HCA II were assessed in the range of pH 5.0−9.0, and those data were compared with the results of ^{18}O exchange catalyzed by H64A HCA II (Figure 4 and Table 3). These data showed only a very small difference between catalysis by H64A/N62H and H64A HCA II (Figure 4). We also assessed catalysis with triple mutant N62H/H64A/N67A that had values of R_{H_2O}/[E] indistinguishable from that of double mutant H64A/N62H HCA II (data not shown). There was a significant enhancement in catalysis for H64A/N67H HCA II at pH <6.5 compared with that of H64A (Figure 4 and Table 3). To estimate the possible contribution of the inserted histidine to catalysis of ^{18}O exchange, we plot the differences $(R_{H_2O}/[E])_{mutant} - (R_{H_2O}/[E])_{H64A}$ in Figure 5. These data show a small enhancement of catalysis for H64A/N62H HCA II amounting to, at most, a contribution that just exceeds 10^3 s^{-1}, but substantial enhancements for H64A/N67H amounting to more than 10^4 s^{-1} for pH values of <6.5 in Figure 5. The solid lines of Figure 5 represent least-squares fits to eq 7, which assumes that the enhancement of R_{H_2O}/[E] above H64A HCA II in the data of Figure 4 is due to proton transfer from the inserted histidine to the zinc-bound hydroxide. The values of R_{H_2O}/[E] of Figure 4 typically have standard errors of up to 20%. Because of the scatter of points and the limited pH range, the parameters of eq 7 presented in Table 3 are often poorly determined.

The data depicted in Figure 6 show the superposition of k_{cat}/K_m for CO_2 hydration for each of the mutants that is being studied here. The values of k_{cat}/K_m for two of the double mutants, H64A/N62H and H64A/N67H, are very similar with those of wild-type and H64A HCA II and serve as a useful control in examining whether the site-specific mutations at residues 62 and 67 have not caused gross structural changes to affect the first stage of catalysis. In Figure 6, the data are fit to a single ionization with pK_a values given in Table 3 and characteristic of the pK_a of the zinc-bound water (*1*). The pK_a values for the zinc-bound water in Table 3 for H64A/N62H and H64A/N67H are in agreement with the values obtained by Liang et al. (*17*) from the pH profile of their esterase activity. In the case of the fit to k_{cat}/K_m for CO_2 hydration catalyzed by H64A/N67H, it appears that a single pK_a is not sufficient to fit the data (Figure 6); here, a second ionization, probably that of His67, is influencing k_{cat}/K_m.

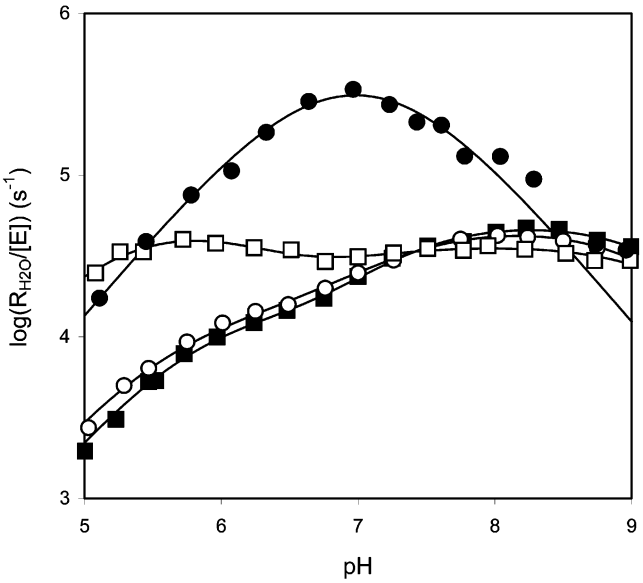

FIGURE 4: pH profiles for R_{H_2O}/[E] catalyzed by wild-type HCA II (●), H64A (■), H64A/N62H (○), and H64A/N67H (□). Data were obtained at 25 °C in the absence of exogenous buffers using a total concentration of all species of CO_2 of 25 mM, with the ionic strength maintained at 0.2 M by addition of sodium sulfate.

Table 3: pH-Independent Rate Constants (maximal values) for Proton Transfer and Apparent Values of pK_a for Histidine as the Proton Shuttle and Zinc-Bound Water in Wild-Type and Mutant HCA II

enzyme	k_B (μs^{-1})[a]	$(pK_a)_{His}$	$(pK_a)_{ZnH_2O}$	Zn−His shuttle distance (Å)
WT[b]	0.8 ± 0.1	7.2 ± 0.1	6.9 ± 0.1	7.5
H64A/N67H	0.2 ± 0.1[c]	5.3 ± 0.3	7.2 ± 0.1	6.6
H64A/N62H	∼0.03[c]	5.7 ± 0.4	7.3 ± 0.1	8.2
H64A	∼0.02	−	6.9 ± 0.1	n/a

[a] Values are from a least-squares fit of eq 7 to the data of Figures 4 and 5. [b] From ref *37*. [c] Values are uncertain due to the scatter of data and the limited pH range.

DISCUSSION

This study has provided an opportunity to comment on the relation between the kinetics of proton transfer and structure in the active site of carbonic anhydrase. We have examined variants of HCA II with histidine residues located at three positions (62, 64, and 67) within the active-site cavity. Crystal structures were determined for pH values of 5.1−10.0 for wild-type HCA II and for pH 6.0 and 7.8 for the two HCA II mutants, H64A/N62H and H64A/N67H. Each of the structures at low pH was observed to have a sulfate ion bound to the zinc (Figures 1−3). This is consistent with the results of Simonsson and Lindskog (*27*) that showed inhibition of catalysis by HCA II at low pH and suggested an interaction of sulfate ions with the zinc ion in the active site. It is interesting that the crystal structures of the sulfate−carbonic anhydrase complexes in each of the variants observed here show sulfate bound to the metal in a mode expected for a protonated inhibitor that is capable of being a hydrogen bond donor in its interaction with the side chain hydroxyl of Thr199 (*28*). These data suggest that the inhibition at low pH by sulfate may be due to binding of a protonated sulfate ion in the mode of other protonated inhibitors such as HSO_3^- and sulfonamides (*28*). Of course, it is also possible that the bound complex involves unprotonated sulfate acting as a hydrogen bond acceptor with the hydroxyl of Thr199. The inferred protonation or hydrogen bonding network can only be resolved by either ultra-high-resolution (>0.8 Å) X-ray crystallography or medium-resolution (∼2.0 Å) neutron crystallography. There are several mutant HCA II structures available that have sulfate bound directly to the zinc ion [PDB entries 1CAI, 1CAJ, and 1CAK(*29*)], but here we report the first structure of wild-type HCA II that shows a sulfate bound to the zinc ion.

For the wild-type HCA II structures at pH 6.1−10.0, there was no sulfate binding evident and two conformations of the side chain of the proton shuttle residue His64 were observed, the in ($\chi_1 = 48°$, $\chi_2 = -98°$) and out ($\chi_1 = -43°$, $\chi_2 = -90°$) conformations (Figures 1 and 7). These data are consistent with the original observation of these two conformations by Nair and Christianson (*9*) that the in (χ_1

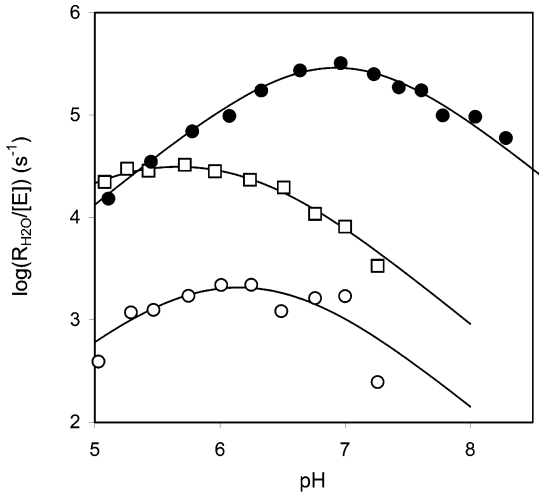

FIGURE 5: pH profiles of the difference $(R_{H_2O}/[E])_{mutant} - (R_{H_2O}/[E])_{H64A}$ for wild-type HCA II (●), H64A/N62H (○), and H64A/N67H (□). Conditions were as described in the legend of Figure 4. The solid lines are least-squares fits of eq 7 to the data with values of parameters given in Table 3.

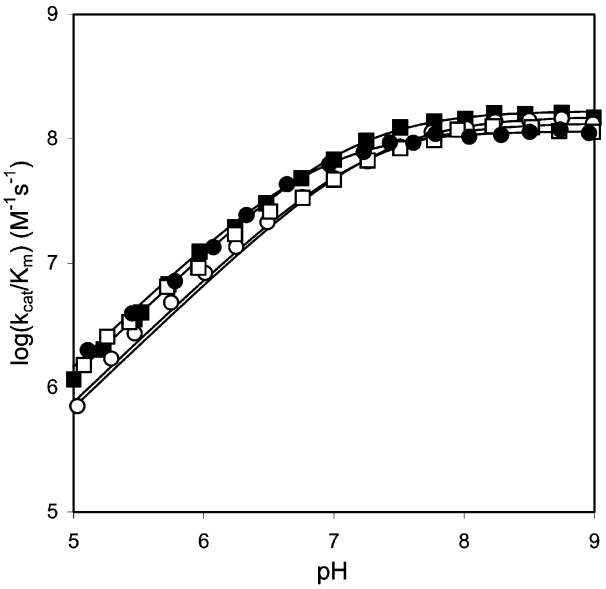

FIGURE 6: pH profiles for k_{cat}/K_m catalyzed by wild-type HCA II (●), H64A (■), H64A/N62H (○), and H64A/N67H (□). Conditions were as described in the legend of Figure 4. The solid lines are fits to a single ionization (eq 6) with the pK_a given in Table 3.

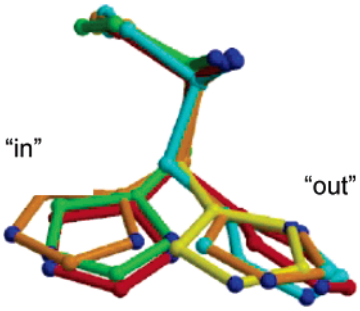

FIGURE 7: Observed rotamer conformations of proton shuttling residue His64 in HCA II. Stick representation of His64: green for the wild type at pH 8.5 [PDB entry 1CA2 (*30*)], yellow for the wild type at pH 5.7 [PDB entry 1CA3 (*9*)], orange for the wild type at pH 6.5 [PDB entry 1HCA (*9*)], red for the wild type at pH 7.0 [PDB entry 1TBT (this paper)], and cyan for the T200S mutant at pH 8.0 [PDB entry 5CA2 (*16*)]. This figure was generated and rendered using BobScript and Raster3D (*34*, *35*).

$= 64°$, $\chi_2 = -101°$) conformation predominates at the more alkaline pH (PDB entries 1HCA and 1CA3 at pH 6.5 and 5.7, respectively; Figure 7), whereas dihedral angle χ_1 for the out ($\chi_1 = -16°$, $\chi_2 = -68°$) conformation from the Nair and Christianson structure at pH 5.7 was different from the angle for the out conformation we observed. This difference could be due to variations in the crystallization buffers that were used. However, the χ_1 observed for the out conformation in our data was similar to those in another structure of HCA II where Thr200 has been replaced with Ser [HCA II T200S (*16*)]. The proton shuttle His64 in this structure also adopts the out ($\chi_1 = -50°$, $\chi_2 = -68°$) conformation (PDB entry 5CA2; Figure 7). We have added to these results the observation that at near-physiological pH we observe both the in and out conformations at near-equivalent occupancies (Figures 1C and 7). This observation is consistent with the function of His64 as the proton shuttle and its physiologic role for catalysis that occurs nearly equally rapidly in hydration and dehydration. That is, in the hydration direction the in conformation of His64 may accept a proton from the zinc-bound water and become the out conformation to deliver the proton to solution, a process which is reversed in dehydration. There is evidence from the binding of 4-methylimidazole to H64A HCA II that the out conformation considered alone is probably not efficient in proton transfer (*18*).

We note, as have others examining HCA II (*9*, *30*), that in the crystal structures there appears to be no completed, hydrogen-bonded water bridge connecting the side chain of His64 with the zinc-bound solvent. The distance from distal water W2, W3A, or W3B to the imidazole ring of His64 exceeds hydrogen bonding distances at each of the pH values that was examined (Figure 1 and Table 2). On the other hand, observation of a completed, hydrogen-bonded water chain between the zinc-bound water and a residue of HCA V alkylated with an imidazole-containing reagent was associated with a very small rate constant for proton transfer [10^3 s^{-1} (*12*, *31*)] compared with that for His64 in HCA II (10^6 s^{-1}). Clearly, observation in the crystal structure of a completed, hydrogen-bonded water link between the proton donor and acceptor in carbonic anhydrase is not a requirement for rapid proton transfer on the scale observed for HCA II. This issue of the nature and existence of hydrogen-bonded solvent networks in the active site will be better resolved by neutron diffraction studies which are ongoing in our laboratory.

The distances between the zinc and the zinc-bound ion (sulfate or OH^-/H_2O) for the wild-type HCA II structures over the pH range that was studied vary from 1.98 to 2.14 Å (Table 2). Previously, Amiss and Gurman (*33*) used EXAFS techniques to investigate Zn−O distances in HCA I from pH 5.0 to 9.0 and reported an average distance of 1.82 ± 0.02 Å that was pH-independent and consistent with an OH^- bound (*33*). Similar EXAFS experiments have shown $Zn-H_2O$ and $Zn-OH^-$ distances to be between 2.00 and 1.85 Å (*32*). The observed distances in the crystal structures of wild-type HCA II in this study are longer than those reported for HCA I (*33*). Extensive kinetic studies of HCA II have shown that the zinc-bound H_2O has a pK_a of ~7, which implies this water ionizes to OH^- at pH >7 (*36*). Therefore, at medium resolution, the crystal structures in this study do not dispute or confirm the presence of a H_2O or OH^- bound at the zinc, and only atomic-resolution X-ray crystallography or neutron diffraction studies could resolve this controversial issue.

We also comment on the proton transfer capabilities of histidine residues placed at two locations in the active-site cavity (62 and 67) that are approximately equivalent to that of His64 in the sense that both have their imidazole rings approximately equidistant from the zinc, 8.2 and 6.6 Å for His62 and His67, respectively; the imidazole side chain of His64 is ~7.5 Å from the zinc ion in wild-type HCA II. Of these, His67 is observed to support proton transfer in catalysis nearly as efficiently as His64 (Table 3). Liang et al. (*17*) using stopped flow to measure initial velocities determined that H64A/N67H HCA II had a value for turnover number k_{cat} that is 20% of that of the wild type, and this work using ^{18}O exchange at chemical equilibrium determined that this mutant had a maximal rate constant for proton transfer that is 25% of that of the wild type (Table 3). On the other hand, the mutant H64A/N62H had a much lower efficiency of proton transfer; in the ^{18}O exchange experiment, the value of the rate constant for proton transfer in H64A/N62H was approximately the same as for mutant H64A HCA II lacking a proton shuttle altogether and was ~25-fold lower than that of the wild type (Table 3). Can the structural data account for these differences? Crystal structures for mutants containing His62 and His67 both show the imidazole side chain extending into the active-site cavity. The imidazole ring of His62 appears to be hydrogen-bonded (a distance of 3.2 Å) with the side chain of Asn67 (Figure 2B), and the imidazole ring of His67 appears to be hydrogen-bonded (distance of 3.0 Å) with the side chain of Asn62 (Figure 3B). However, there is one difference in structure that may be significant. The side chain of His67 is connected to the zinc-bound solvent molecule by a completed, hydrogen-bonded chain containing two water molecules (W1 and W2 of Figure 3B, Table 2). The His62 side chain requires three water molecules to span this distance (W1, W2, and W3B of Figure 2B; Table 2). Actually, in the cases of both His67 and His62, the crystallography implies a very weak hydrogen bond (3.2 Å) between the distal water (W2 or W3B) and the imidazole side chain of His64 (Table 2). Since we have surmised that a completed, hydrogen-bonded water chain in the crystal structure does not necessarily associate with efficient proton

transfer, the closer distance spanned by two water molecules from His67 to the zinc-bound solvent may be more significant. We note that the apparent hydrogen bond between the side chain of His67 and Asn62 (Figure 3B) does not preclude efficient proton transfer. This indicates that proton shuttle residue His67 still sustains appreciable proton transfer rates even though its side chain is involved in a hydrogen bonding interaction that could restrict its mobility.

In summary, the side chain of the critical proton shuttle residue His64 has two side chain conformational states approximately equally populated at physiological pH. There is no completed, hydrogen-bonded water chain in the crystal structure associated with this efficient proton transfer. The features for an efficient proton shuttle are attained for His67 in contrast with the inefficient His62. In these examples, the distance spanned by the proton transfer appears to be more significant for efficient proton transfer than the observation of a complete, hydrogen-bonded water chain in the crystal structure. These data suggest that in HCA II two intervening water molecules between the donor and acceptor is consistent with an efficient proton transfer. Cui and Karplus (*7*) reached this conclusion for carbonic anhydrase using density functional calculations and give a theoretical basis for this conclusion.

ACKNOWLEDGMENT

We thank Professor Sven Lindskog for providing the two double mutants used in this work. We thank Max Iurcovich for excellent technical assistance.

REFERENCES

1. Lindskog, S. (1997) Structure and mechanism of carbonic anhydrase, *Pharmacol. Ther. 74*, 1−20.
2. Christianson, D. W., and Fierke, C. A. (1996) Carbonic Anhydrase: Evolution of the Zinc Binding Site by Nature and by Design, *Acc. Chem. Res. 29*, 331−339.
3. Silverman, D. N., and Lindskog, S. (1988) The catalytic mechanism of carbonic anhydrase: Implications of a rate-limiting protolysis of water, *Acc. Chem. Res. 21*, 30−36.
4. Tu, C. K., Silverman, D. N., Forsman, C., Jonsson, B.-H., and Lindskog, S. (1989) Role of histidine 64 in the catalytic mechanism of human carbonic anhydrase II studied with a site-specific mutant, *Biochemistry 28*, 7913−7918.
5. Venkatasubban, K. S., and Silverman, D. N. (1980) Carbon dioxide hydration activity of carbonic anhydrase in mixtures of water and deuterium oxide, *Biochemistry 19*, 4984−4989.
6. Smedarchina, Z., Siebrand, W., Fernandez-Ramos, A., and Cui, Q. (2003) Kinetic isotope effects for concerted multiple proton transfer: A direct dynamics study of an active-site model of carbonic anhydrase II, *J. Am. Chem. Soc. 125*, 243−251.
7. Cui, Q., and Karplus, M. (2002) Quantum mechanics/molecular mechanics studies of triosephosphate isomerase-catalyzed reactions: Effect of geometry and tunneling on proton-transfer rate constants, *J. Am. Chem. Soc. 124*, 3093−3124.
8. Silverman, D. N., Tu, C., Chen, X., Tanhauser, S. M., Kresge, A. J., and Laipis, P. J. (1993) Rate-equilibria relationships in intramolecular proton transfer in human carbonic anhydrase III, *Biochemistry 32*, 10757−10762.
9. Nair, S. K., and Christianson, D. W. (1991) Unexpected pH-dependent conformation of His-64, the proton shuttle of carbonic anhydrase II, *J. Am. Chem. Soc. 113*, 9455−9458.
10. Tripp, B. C., and Ferry, J. G. (2000) A structure−function study of a proton transport pathway in the γ-class carbonic anhydrase from *Methanosarcina thermophila*, *Biochemistry 39*, 9232−9240.
11. Iverson, T. M., Alber, B. E., Kisker, C., Ferry, J. G., and Rees, D. C. (2000) A closer look at the active site of γ-class carbonic anhydrases: High-resolution crystallographic studies of the carbonic anhydrase from *Methanosarcina thermophila*, *Biochemistry 39*, 9222−9231.
12. Jude, K. M., Wright, S. K., Tu, C. K., Silverman, D. N., Viola, R. E., and Christianson, D. W. (2002) Crystal structure of F65A/Y131C-methylimidazole carbonic anhydrase V reveals architectural features of an engineered proton shuttle, *Biochemistry 41*, 2485−2491.
13. Khalifah, R. G. (1971) The carbon dioxide hydration activity of carbonic anhydrase. I. Stop-flow kinetic studies on the native human isoenzymes B and C, *J. Biol. Chem. 246*, 2561−2573.
14. Steiner, H., Jonsson, B.-H., and Lindskog, S. (1975) The catalytic mechanism of carbonic anhydrase. Hydrogen-isotope effects on the kinetic parameters of the human C isoenzyme, *Eur. J. Biochem. 59*, 253−259.
15. Campbell, I. D., Lindskog, S., and White, A. L. (1975) A study of the histidine residues of human carbonic anhydrase C using 270 MHz proton magnetic resonance, *J. Mol. Biol. 98*, 597−614.
16. Krebs, J. F., Fierke, C. A., Alexander, R. S., and Christianson, D. W. (1991) Conformational mobility of His-64 in the Thr-200 → Ser mutant of human carbonic anhydrase II, *Biochemistry 30*, 9153−9160.
17. Liang, Z., Jonsson, B.-H., and Lindskog, S. (1993) Proton transfer in the catalytic mechanism of carbonic anhydrase. Effects of placing histidine residues at various positions in the active site of human isoenzyme II, *Biochim. Biophys. Acta 1203*, 142−146.
18. An, H., Tu, C. K., Ren, K., Laipis, P. J., and Silverman, D. N. (2002) Proton transfer within the active-site cavity of carbonic anhydrase III, *Biochim. Biophys. Acta 1599*, 21−27.
19. Khalifah, R. G., Strader, D. J., Bryant, S. H., and Gibson, S. M. (1977) Carbon-13 nuclear magnetic resonance probe of active-site ionizations in human carbonic anhydrase B, *Biochemistry 16*, 2241−2247.
20. McPherson, A. (1982) *Preparation and Analysis of Protein Crystals*, Wiley, New York.
21. Otwinowski, Z., and Minor, W. (1997) Processing of X-ray Diffraction Data Collected in Oscillation Mode, *Methods Enzymol. 276*, 307−326.
22. Jones, T. A., Zou, J. Y., Cowan, S. W., and Kjeldgaard, M. (1991) Improved methods for building protein models in electron density maps and the location of errors in these models, *Acta Crystallogr. A47*, 110−119.
23. Brünger, A. T., Adams, P. D., Clore, G. M., DeLano, W. L., Gros, P., Grosse-Kuntsleve, R. W., Jiang, J. S., Kuszewski, J., Nilges, M., Pannu, N. S., Read, R. J., Rice, L. M., Simonson, T., and Warren, G. L. (1998) Crystallography & NMR system: A new software suite for macromolecular structure determination, *Acta Crystallogr. D54*, 905−921.
24. Håkansson, K., Carlsson, M., Svensson, L. A., and Liljas, A. (1992) Structure of native and apo carbonic anhydrase II and structure of some of its anion-ligand complexes, *J. Mol. Biol. 227*, 1192−1204.
25. Silverman, D. N. (1982) Carbonic anhydrase:oxygen-18 exchange catalyzed by an enzyme with rate-contributing proton-transfer steps, *Methods Enzymol. 87*, 732−752.
26. Krebs, J. F., Ippolito, J. A., Christianson, D. W., and Fierke, C. A. (1993) Structural and functional importance of a conserved hydrogen bond network in human carbonic anhydrase II, *J. Biol. Chem. 268*, 27458−27466.
27. Simonsson, I., and Lindskog, S. (1982) The interaction of sulfate with carbonic anhydrase, *Eur. J. Biochem. 123*, 29−36.
28. Liljas, A., Håkansson, K., Jonsson, B.-H., and Xue, Y. (1994) Inhibition and catalysis of carbonic anhydrase. Recent crystallographic analyses, *Eur. J. Biochem. 219*, 1−10.
29. Xue, Y., Liljas, A., Jonsson, B.-H., and Lindskog, S. (1993) Structural analysis of the zinc hydroxide-Thr-199-Glu-106 hydrogen-bond network in human carbonic anhydrase II, *Proteins 17*, 93−106.
30. Eriksson, A. E., Jones, T. A., and Liljas, A. (1988) Refined structure of human carbonic anhydrase II at 2.0 Å resolution, *Proteins 4*, 274−282.
31. Earnhardt, J. N., Wright, S. K., Qian, M., Tu, C. K., Laipis, P. J., Viola, R. E., and Silverman, D. N. (1999) Introduction of histidine analogs leads to enhanced proton transfer in carbonic anhydrase V, *Arch. Biochem. Biophys. 361*, 264−270.
32. Bergquist, C., Fillebeen, T., Morlok, M. M., and Parkin, G. J. (2003) Protonation and reactivity towards carbon dioxide of the mononuclear tetrahedral zinc and cobalt hydroxide complexes, [$Tp^{Bu^t,Me}$]ZnOH and [$Tp^{Bu^t,Me}$]CoOH: Comparison of the reactivity of the metal hydroxide function in synthetic analogues of carbonic anhydrase, *J. Am. Chem. Soc. 125*, 6189−6199.

33. Amiss, J. C., and Gurman, S. J. (1999) Biological EXAFS at room temperature, *J. Synchrotron Radiat. 6*, 387−388.
34. Merrit, E. A., and Bacon, D. J. (1997) Raster3D: Photorealistic Molecular Graphics, *Methods Enzymol. 277*, 505−524.
35. Esnouf, R. M. (1999) Further additions to MolScript version 1.4, including reading and contouring of electron-density maps, *Acta Crystallogr. D55*, 938−940.
36. Lindskog, S., and Silverman, D. N. (2000) The catalytic mechanism of mammalian carbonic anhydrases, in *The Carbonic Anhydrases: New Horizons* (Chegwidden, W. R., Carter, N. D., and Edwards, Y. H., Eds.) pp 175−195, Birkhäuser Verlag, Basel, Switzerland.
37. Duda, D. M., Tu, C. K., Qian, M., Laipis, P. J., Agbandje-McKenna, M., Silverman, D. N., and McKenna, R. (2001) Structural and kinetic analysis of the chemical rescue of the proton transfer function of carbonic anhydrase II, *Biochemistry 40*, 1741−1748.

BI0480279